THE HYDROGEN LINE IN ABSORPTION

B. G. Clark, V. Radhakrishnan, and R. W. Wilson
California Institute of Technology, Radio Observatory
Received August 19, 1961

ABSTRACT

21-cm absorption spectra have been obtained for twelve radio sources, using conventional techniques. Six of these sources were also studied with a hydrogen-line interferometer. Differences in the profiles obtained by the two methods give information on the structure and temperature of the H I clouds seen in absorption Estimates of the angular sizes of four clouds based on these differences lead to an average diameter of 13 parsecs. In some cases it has been possible to find an upper limit to the temperature of the clouds somewhat lower than the generally assumed 125° K. A temperature of 60° K is suggested, giving densities of 20 atoms/cc and masses of $10^3\ M\odot$ for the absorbing clouds.

I. INTRODUCTION

As part of a general program comprising both the determination of distances to radio sources and the study of galactic structure, 21-cm absorption measurements were started at the Owens Valley Radio Observatory in 1959. One of the observatory's two 90-foot paraboloids was used with a frequency comparison receiver having a band width of 6 kc/sec to study a number of galactic sources (Radhakrishnan and Bolton 1960). Two main difficulties were encountered in this investigation: one was the determination of the expected profile, and the other was the accurate measurement of large optical depths. Subsequent improvements in technique, dealt with in the next section, have made it possible to obtain reasonable absorption profiles for about a dozen radio sources. The detailed results and discussion thereof are presented in succeeding sections, and the rest of this section is devoted to a brief review of some of the previous work in this field.

The first observation of 21-cm absorption was made by Hagen and McClain (1954), who found that if a comparison-type radiometer was tuned to a peak in the hydrogen spectrum and the antenna swept through the position of a strong radio source, there was a sharp decrease in the observed intensity at the position of the source. It soon became clear that the interstellar hydrogen in front of the continuum source was producing an absorption line in the spectrum of the source similar to those formed in the optical range by interstellar calcium and sodium. In a later paper Hagen, Lilley, and McClain (1955) first outlined the two now well-accepted methods of obtaining an absorption profile with a single antenna and treated the theory and physical significance of the observations in detail. From measurements on the radio source Cassiopeia A, made with a 5 kc/sec band width, it was shown that a cloud model for the distribution of the interstellar hydrogen was necessary to explain the striking dissimilarities between the absorption profile for the source and the emission profile obtained in neighboring directions. A minimum distance for the Cassiopeia source was also determined following a method outlined by Williams and Davies (1954).

Using a 25-meter paraboloid and a 5 kc/sec band width, Muller (1957, 1958) obtained absorption profiles for five strong sources of small diameter. He was able to reduce the error in determining the expected profile by scanning across some of the sources at constant galactic latitude. Muller's results amply confirmed the earlier NRL evidence of cloud structure in the hydrogen and showed that the r.m.s. velocity in the clouds was, in general, much higher than expected from thermal broadening alone, indicating mass motions inside the clouds. One of the three major components in the Cas A spectrum was found to have a surprisingly high optical depth of $\tau = 4$.

In addition to absorption in the spectra of discrete sources, there are also self-absorp-

tion effects. Heeschen (1955), Davies (1958), and Radhakrishnan (1960) have all reported evidence of the absorption of background emission by hydrogen clouds at temperatures well below the usual 125° K found from emission observations. There would seem to be little doubt that extended 21-cm absorption studies offer the most promising way of investigating the temperature, density, and velocity distribution of the interstellar medium.

II. THE TECHNIQUE OF ABSORPTION MEASUREMENTS

The formulae for describing single-dish absorption measurements were first given by Hagen *et al.* (1955). If we turn the antenna in the direction of a source which has hydrogen clouds around it, the response of a frequency-comparison receiver is given by

$$R \propto \langle \Delta T(\nu) \rangle - T_A \{ 1 - \exp [- \tau(\nu)] \}, \quad (1)$$

where $\langle \Delta T(\nu) \rangle$ is the mean brightness temperature of all the H I clouds in the beam of the antenna weighted by the antenna pattern (this is often called the expected profile); T_A

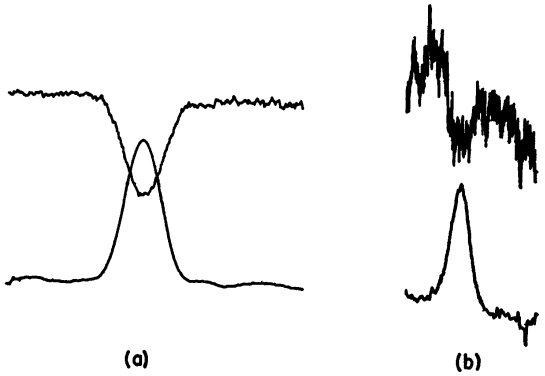

FIG. 1.—Drift-curves in right ascension of (*a*) Cassiopeia A and (*b*) Westerhout 51 showing absorption. The upper trace is the output of the narrow-band (6 kc/sec) frequency comparison receiver, and the lower trace is the output of a broad-band d.c. radiometer. The temperature scales are roughly equivalent in the two channels in both figures. The change in background temperature with position in the sky is more marked in the case of W51.

is the temperature of the source weighted in the same manner; and $\tau(\nu)$ is the optical depth of the clouds between us and the source—$e^{-\tau(\nu)}$ is averaged over the source distribution at the frequency ν. The intrinsic temperature of most radio sources outside the solar system is 10000° K or more, while the brightness temperature of H I regions is of the order of 100° K. The effect of the source absorbing line radiation originating from behind can therefore be shown to be about 1 per cent or less of the source intensity. We have consequently neglected this effect.

In Figure 1 are two curves showing absorption in the spectra of Cassiopeia A and Westerhout 51. They were obtained with a frequency-comparison receiver which produces a downward deflection (*upper trace*) at the position of the source in the presence of absorption. The lower traces are from a continuum receiver and serve mainly to indicate the position of the source.

In comparison-receiver observations, the line-receiver deflection corresponding to the full-source intensity, T_A, must be found by some auxiliary method, since the receiver responds to T_A only in proportion to the amount it is absorbed. For large optical depths a small error in the determination of this deflection (caused perhaps by a small gain change) will cause a large error in the value of τ.

A more straightforward solution to the determination of τ in these cases is to observe

with an unswitched, single-sideband, narrow-band receiver (Fig. 2). The output of the receiver is now given by

$$R \propto \langle \Delta T(\nu) \rangle + T_A \exp [- \tau(\nu)] . \quad (2)$$

If we tune the receiver to a frequency outside the range of line emission or absorption (Fig. 2, *a*, *d*), the response to T_A can be measured by sweeping the antenna across the source. The absorption will be measured as a reduction in the source response for certain frequencies (Fig. 2, *b*, *c*, *e*). Where there is considerable absorption, the remaining response to the source will not be large, and small gain changes will have only a negligible effect. Where there is little absorption, however, we are again taking the difference of

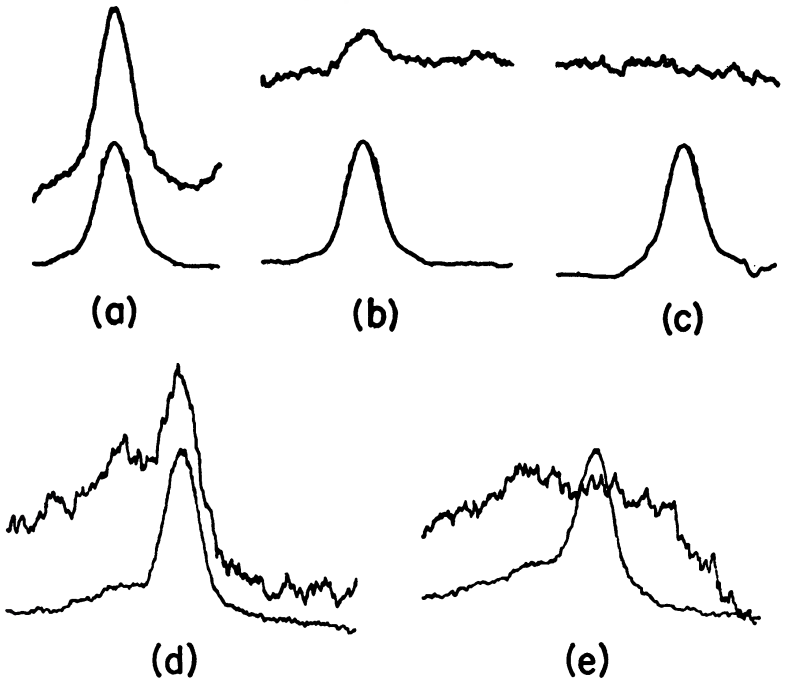

FIG. 2.—Drift-curves at different frequencies taken with a single-sideband d.c receiver showing absorption. Upper trace in each figure is the movable 6 kc/sec channel and the lower trace the fixed 5 Mc/s channel. The top figures show Cassiopeia A (*a*) unabsorbed, (*b*) partly absorbed halfway down the deep line, and (*c*) at the bottom of the deep line. The bottom figures show the Omega Nebula (*d*) superimposed on the H I emission from the galaxy and (*e*) in a deep absorption line.

two large quantities, and the effect of small gain changes will be to cause a relatively large error in τ. This form of receiver is, of course, subject to the usual instability of output zero level associated with d.c. receivers. We have therefore used the switched receiver to find weak absorption and the unswitched receiver to measure accurately deep absorption features.

To obtain $\tau(\nu)$, which is the true absorption spectrum of the radio source, it is still necessary to separate the source from the background of hydrogen emission within the beam of the antenna. The latter is often many times larger than the angular dimensions of the continuum source. The two usual methods of deriving $\langle \Delta T(\nu) \rangle$ (the expected profile) are both based on interpolation between neighboring regions of the sky. In the frequency-scanning method, profiles are taken with the antenna tracking each of a number of points around the position of the source in question, and these profiles are then averaged together to obtain a mean. In the other method dealt with above, the receiver is set at a fixed frequency and the antenna beam moved across the position of the source

in right ascension or in declination (Figs. 1 and 2). The recorder trace is then interpolated across the position of the source, to give the value of the expected profile at that particular frequency. In the case of Cas A (Figs. 1, *a*, and 2, *a*, *b*, *c*) the interpolation seems straightforward, as the background is varying very slowly, whereas for W51 (Fig. 1, *b*) and M17 (Fig. 2, *d*, *e*) the rapid change in the background is quite evident. The important point to bear in mind is that, with either the frequency-scanning method or the drift-curve method, the expected profile has to be interpolated between regions at least a full *beam width* away. Thus the high resolution that is expected from absorption measurements—that of the diameter of the source—cannot be fully realized.

The problem of the expected profile was also approached with two new methods. In the first, a frequency scan taken with our 90-foot antenna at the position of a source was compared with one taken at the same position with a 25-foot antenna. A small diameter source would produce about a tenth of the temperature in the smaller antenna as it would in the larger one, and the absorption features in the observed profile would be proportionally weaker. It was assumed that the difference between the two profiles would be

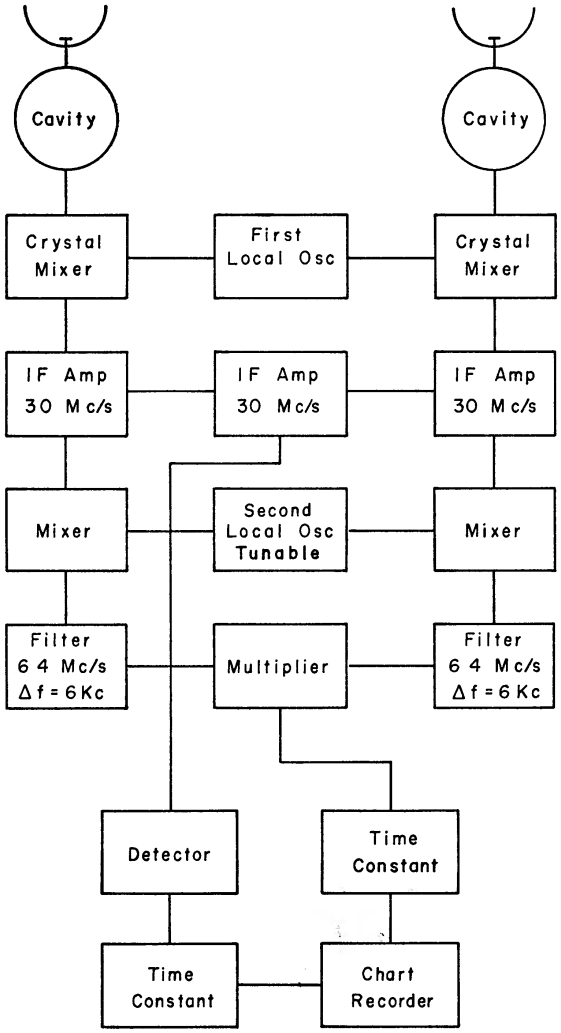

FIG. 3.—A block diagram of the hydrogen-line interferometer. For a single-dish d.c. radiometer operation, one of the two halves of the interferometer was used with an ordinary detector replacing the multiplier.

essentially the absorption spectrum of the source times a scale factor. As might be expected, this method proved unsuccessful. The smaller dish averaged variations in the emission background over a region ten times the solid angle subtended by the smaller beam of the larger antenna, and this was apparently somewhat different from the background right at the position of the source.

The other approach, which proved very fruitful, was to use the two 90-foot antennas together in an interferometer arrangement (Radhakrishnan, Morris, and Wilson 1960). They were separated by 300 wavelengths along an east-west base line and were connected together as indicated in the block diagram of Figure 3. The interferometer had two outputs, a broad-band total-power output and a narrow-band multiplier output from a 6 kc/sec channel. The position of the narrow channel within the broad band could be varied by tuning the second local oscillator. Both outputs were displayed on the same chart (Fig. 4) and correspond to the single-dish line and continuum traces as seen in Figures 1 and 2. The bottom trace shows a gentle attenuation from left to right due to the effect of the accumulating path difference with increasing hour angle on the wide band width but is otherwise of constant amplitude. The top trace shows drastic variations in

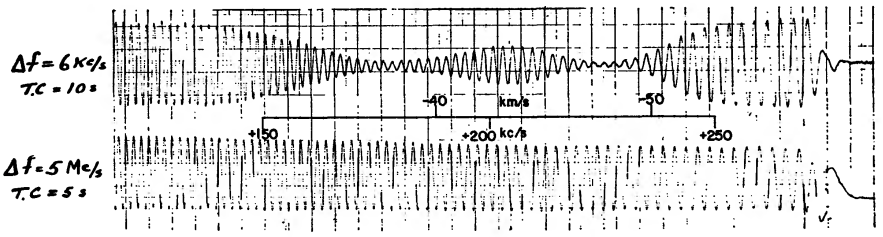

FIG. 4.—An interferometer measurement of part of the absorption spectrum of Cassiopeia A. Upper trace shows the narrow-band multiplier output as the receiver is tuned through the two deep lines caused by clouds in the Perseus arm (Fig. 6, *A*) Lower trace is the broad-band total-power output, showing a slight effect of band-width attenuation with increasing delay in one arm of the interferometer. Noise level is seen at extreme right, where the antennas were moved off the source.

amplitude as the narrow-band filters are tuned through the frequency range of the two deep features in the absorption spectrum of Cassiopeia. The signal-to-noise ratio can be estimated from the right-hand end of the top trace, where the antennas were moved off the source.

The principle behind the interferometer method is the following. The amplitude of the fringes produced by a small-diameter source at any frequency is independent of the spacing of the antennas, until the lobe separation approaches the size of the source and the interferometer begins to resolve it. The background emission, on the other hand, having in general a lower brightness temperature than the source and a structure gross compared with that of the source, is resolved out and produces no fringe pattern. If the interferometer is swept in frequency through the hydrogen spectrum, the narrow-band fringes will have an amplitude proportional to the transparency of the hydrogen in front of the source at each frequency. If A is the amplitude outside the hydrogen band, then $A_\nu = A^{e-\tau(\nu)}$ is the fringe amplitude at frequency ν. Thus $\tau(\nu)$ is directly determined and the expected profile made redundant. For a point source, any observed difference between the single-dish and the interferometer absorption profiles can be due only to an error in the single-dish expected profile caused by structure in the emission roughly coincident with the source position. From the differences between the two profiles, one may determine the nature of the structure, and this is what we have done.

According to the simple picture outlined above, the multiplying interferometer interpolates and subtracts the background between regions a lobe separation apart, thus providing greater accuracy than when dealing with regions at least two beam widths apart,

as in single-dish techniques. If antenna movement permits, the lobe spacing can be decreased arbitrarily for point sources, giving greater and greater accuracy in finding the true absorption profile. However, two factors complicate the interferometer method and, at the same time, increase its potentialities. The first is that hydrogen emission alone will produce fringes having an amplitude and phase appropriate to the spatial frequency components in the brightness distribution to which the interferometer is sensitive. As far as is known, no high-resolution investigation of the fine structure of the hydrogen emission has been done so far, mainly for lack of suitable instruments. The second factor is that most of the strong sources in the galaxy begin to be resolved even at moderate interferometer spacings of a few hundred wavelengths, and great difficulties are introduced into the interpretation of the observations.

The observed fringes are the vector sum of the fringes produced by the emission alone and those produced by the source modified by the absorption. Hence any change in the apparent absorption profile with resolution can be explained, in general, either in terms of a structure in the hydrogen in front of the source or in the emission anywhere within the primary beam. To extract the maximum amount of information, one must compare the brightness distribution over the source at all frequencies of interest with that outside the hydrogen spectrum. However, one must still interpolate the expected profile across the source, in order to determine the true absorption. Thus, if there is structure in the hydrogen emission within the solid angle subtended by the continuum source, then, in principle, it will not be possible uniquely to determine the distribution of τ and T_k by absorption studies.

Appropriate equations for the quantities measured with the interferometer method are given in the Appendix.

No attempt was made to measure the phase of the interferometer fringes or its change as a function of frequency. In the reduction and interpretation of the results presented here, very simple models have been assumed. Discrepancies between single-dish and interferometer spectra are explained in terms of single clouds situated in front of the source. A suitable combination of angular size and brightness temperature was chosen to fit the observations.

III. THE OBSERVATIONS

The true absorption profiles, obtained as described above, were corrected for the finite band width of the receiver by the chord correction method of Bracewell (1955). For those sources with a very complicated absorption spectrum, the profile was plotted on a scale linear in optical depth and was divided by eye into separate features with plausibly shaped profiles, always with the restriction that the sum of the individual profiles must yield the observed profile. As an example of this sort of plot, the interferometer profile for the source M17 is shown in Figure 5. This procedure is quite susceptible to error when the features are closely blended, and we have tried to indicate this in our estimated errors. The width of shallow lines is especially difficult to judge when they occur near deep lines.

The errors quoted were estimated from the consistency of various observations of the same feature. The difference between adjacent values may have less error than the curve as a whole. For this reason we feel justified in including kinks in our profiles of height about equal to the estimated error. The errors do not include systematic effects caused, for example, by local variations in the hydrogen emission. There has been no attempt to reduce this type of error by, for instance, taking drift-curves in declination. The absolute error in frequency measured by the receiver probably amounts to about 2 kc/sec. However, the reading error from the curves may be much greater, especially in the case of the blended features. The error in the half-widths of the lines is almost entirely due to improper separation of blended components and to uncertainty in the maximum optical depth.

We have not ourselves directly observed the expected profile; however, in order to indicate the hydrogen emission in the region of interest, an approximate expected profile is included. For the strong sources—all those observed with both the single dish and the interferometer and for W51—the expected profile was taken by B. Höglund at the Chalmers Institute of Technology. These profiles were obtained with a small dish (7.5 meters in diameter) pointing at the source position. In this case the source makes a small contribution to the antenna temperature, so that the absorption, which at most amounts to the antenna temperature of the source, is nearly negligible. The profiles were taken with a band width of approximately 30 kc/sec and are presented uncorrected for band width.

The following figures (6–11) present the results of our observations. The top part of each figure is the expected profile, the second part is the profile obtained with the single dish (35′ beam width), and the third, the profile as obtained with the interferometer (12′ east-west lobe spacing). In the cases where the band-width correction amounts to an

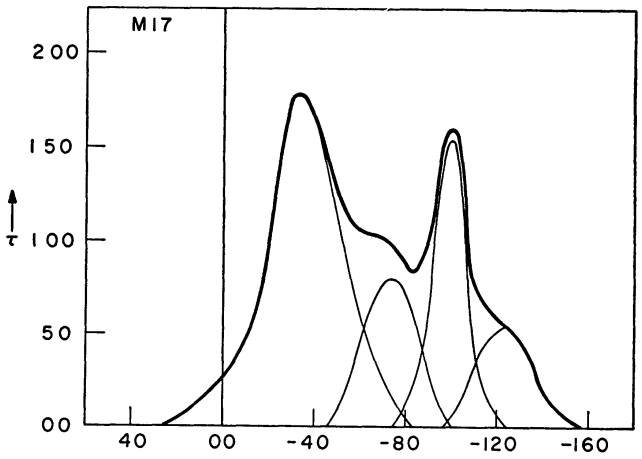

FIG. 5.—The interferometer absorption profile for the Omega Nebula plotted on a scale linear in τ for separating the components.

appreciable part of the estimated error, the uncorrected profile is also included as a dotted line. The estimated error in the profile is indicated on the figure. As the percentage error depends on the amount of absorption and on the number of observations made of the source, several error bars may be indicated on each profile, each applying to the nearby portion of the profile at about the same height as the error bar. Where there is only one error bar, it applies to the entire profile.

Table 1 lists the sources observed. The first column names the source. "W" and "3C" refer to the Westerhout (1958) and the third Cambridge survey (Edge, Shakeshaft, McAdams, Baldwin, and Archer 1959) catalogues. In the second and third columns are given the positions in the new galactic co-ordinates. The fourth column gives the optical identification of the object, where such identification exists. We have also listed a distance derived from the identification in the same column. In the fifth column is the intensity of the source as observed with a single dish, expressed as a ratio to Cas A. The sixth and seventh columns indicate the approximate angular size of the object and the fringe visibility with an interferometer of 300 wavelength east-west spacing. In the eighth column are the frequencies searched for absorption. The ninth and tenth columns pertain to the determination of the distance of the source. In the tenth column is listed the kinematical distance of the most distant feature in the absorption spectrum, and in the ninth column is given the frequency at which this feature occurs. (The frequencies and distances are found in Table 2.) The eleventh and twelfth columns list the frequency and kinematical distance of the nearest feature in the emission profile which does not

appear in absorption. The source is not necessarily in front of the emission feature, as there may be a gap in the hydrogen through which the source appears. This apparently occurs for some of the emission in the direction of the Cygnus source.

The individual features are listed in Table 2. The first column lists the source, and the second and third the center frequency of the absorption feature and the corresponding radial velocity. The next three columns present the single-dish results. The fourth column lists the maximum optical depth in the feature, along with the appropriate error. The fifth column indicates the full width at half optical depth, expressed in kilocycles per

TABLE 1

SOURCES OBSERVED FOR ABSORPTION

Source	l^{II}	b^{II}	Optical Identification Type Dist (kpc)	Intensity I/I Cas	Approx Fringe		Frequencies Searched (kc/sec)		Most Distant Absorption Feature		Nearest Unabsorbed Emission Feature	
					Size	Vis	From	To	kc/sec	r (kpc)	kc/sec	r (kpc)
(1)	(2)	(3)	(4)	(5)	(6)	(7)	(8)		(9)	(10)	(11)	(12)
Cas A	111 51	− 0 22	Supernova 3	1 00	5′	0 75	−100	+400	+229	3 8	+460	7 5
Cygnus A	76 50	+ 5 75	Galaxy . .	0 61	1.′4	0 90	−200	+600	+446	10 9		
Crab Neb	184 53	− 5 79	Supernova 1 1	0 36	4′	0 75	−100	+ 50	...	...	...	...
Orion Neb.	209 08	−19 26	Em Neb 0 5	0 17	7′	0 45	−120	+ 60	− 38	0 47	− 49	0 62
Omega Neb	14 95	− 0 72	Em. Neb M17, NGC 6618	0 23	6.′5	0 4	−230	+130	−124	2 6	−190	3 7
Sgr A	0	− 0 15	Galactic, center 8 2	0 42	1°*	0 22	−200	+360	...	...		
3C 123.	170 58	−11 41		0 025	<1′	1 00	− 80	+ 80	− 22	0		
CTB 31.	267 88	− 1 06		0 064	30′×15′		− 50	+ 50	− 23	0 9	− 80	2 3
CTB 34†	335 76	+ 2 37	. . .	0 059	0°.8		− 50	+500				
CTB 39	349 76	+ 2 50	Em. Neb NGC 6334	0 055	12′		− 80	+300	+ 27	0 8		
W22	353 23	+ 0 43	Em. Neb NGC 6357 1	0 16	36′		−125	+125				
W28‡	6 36	− 0 12		0 058	15′×48′		−150	+250	...	...		
W43	30 70	+ 0 83		0 082	15′		−600	+150	−445	5 9, 9 3		
W51	49 10	− 0 40		0 10	18′		−500	+ 50	−260	4 4, 6 3	+220	13 4
W75	81 55	+ 0 36		0 035	2°		− 65	0	− 54	1 2	+100	4 5

* The source consists of two components The size 1° is appropriate to the single-dish observation With the interferometer, almost all the source is resolved out except a core of about 3.′5

† There appear to be no absorption features in the spectrum of CTB 34 with optical depth greater than 1 in the range observed. CTB numbers are from Wilson and Bolton (1960)

‡ W28 probably has an absorption feature between −20 and −40 kc/sec, with an optical depth less than 0 8

second. The sixth column gives $\int \tau dv$, where the integration is carried out over the feature in question. To obtain the number of atoms per square centimeter in the line of sight, one multiplies this number by the constant $3.88 \times 10^{17}\ T$. We prefer to give this quantity instead of the number of atoms in the line of sight because the temperature of these clouds is not well known. The next three columns give the same information obtained with the interferometer. The last column of the table gives the kinematical distance to the cloud forming the feature. All the above kinematical distances are based on the rotation curves derived by Schmidt (1956). In the ambiguous cases, both possible distances are given. If one seems much less likely than the other, it is inclosed in parentheses. Table 3 continues Table 2 for those sources observed only with the single dish.

a) Cassiopeia A

The absorption profiles for Cassiopeia A are shown in Figure 6. The most obvious features in the spectrum of this source are the three very deep and narrow lines, two of which have velocities corresponding to the Perseus arm and one the Orion arm. There are several other features of much lower optical depth at intermediate frequencies. There is some suggestion that the strong features may be resolved into finer structure. Muller

TABLE 2

ABSORPTION FEATURES OBSERVED WITH THE INTERFEROMETER

Source	Freq (kc/sec)	Vel. (km/sec)	Single Dish			Interferometer			τ (kpc)
			Max τ	Width	Int τ	Max τ	Width	Int τ	
(1)	(2)	(3)	(4)	(5)	(6)	(7)	(8)	(9)	(10)
Cas A	− 36	+ 7 6	0 08 ±0 06	15?	1 6	0 13±0 05	24	2 8	0
	+ 4	− 0 8	1 98 ± 12	15	33	2 00±0 12	17	35	0 1
	+ 28	− 5 9	0 18 ± .06	15?	2 6	. . . . .	. . .	. .	0 6
	+ 64	−13 5	0 05 ± 06	30?	1 4	0 09±0 05	12?	1 4	1 0
	+180	−38 0	3 10 ± 2	31	98	2 53±0 25	32	79	3 0
	+229	−48 3	>4 7	≈16*	≈88	3 41±0 4	22	74	3 8
Cyg A	− 14	+ 3 0	0 25 ± 06	45	11	0 29±0 06	50	16	0 38 (3 4)
	+ 54	−11 4	.			0 08±0 06	27	2 8	4 7
	+ 95?	−20 1	. . . .	. .	. .	0 04±0 06	?	1 0	5 4
	+344	−72 6	0 09 ± 06	18?	1 8	. . . .	. .		9 2
	+403	−85 1	0 22 ± 06	28	6 3	0 18±0 06	23	4 6	10 1
	+446	−94 1	0 05 ± 06	?	0 7	0 03±0 06	?	0 5	10 9
Crab Neb	+ 3	− 0 6	0 21 08	15	3 7	0 24±0 07	13	4 6	. .
	− 10	+ 2 1	0 53?± 3						. .
	− 20	+ 4 2	0 68?± 3	.		. . . .	.	.	. . . . .
	− 15†	+ 3 2	0 70 ± 10	25	18	0 72±0 07	20	12	. . . . .
	− 28	+ 5 9	.	. .	.	0 5?±0 4	?	5?	. . . . .
	− 48	+10 1	1 56 + 4 − 3	13	22	1 05±0 2	13	16	. . . . .
Orion Neb	− 38	+ 8 0				0 60±0 25	9	9 1	0 47
	− 24	+ 5 1				2 4 +1 2 −0 6	14	43	0 27
	− 19	+ 4 0	1 27 ± 25	27	46	. . . . .	. . .	. .	0 22
	− 11	+ 2 3			.	1 25±0 35	10	16	0 11
	− 1	+ 0 2	. . .	. .	.	0 63±0 25	10	7 6	0
	+ 4	− 0 8	0 36 ± 15	13?	5 7	. . . .	. .	.	0
	+ 14‡	− 3 0	0 15 ± 10	≈10	2 0	0 25±0 15	12	6	0
Omega Neb	+ 24	− 5 1	0 25?± 15	. . .	. .			.	0 (15.8)
	− 7	+ 1 5	0 78?± 4	21?	18?	. . . .	.	. .	0 16(15 6)
	− 34§	+ 7 2	1 70 ± 28	35?	56	1 77±0 22	35	72	0 73(15.1)
	− 73	+15 4	1 4 ± 5	25?	35?	0 82±0 30	30?	23?	1 6(14 2)
	−100	+21 1	3 2 + ∞ − 9	25	80	1 61±0 20	17	29	2 1(13 7)
	−124	+26 2	0 92 ±0 3	30	27	0 54±0 3	30	15	2 6(13 2)
Sgr A ..	+253	−53 4			.	1 05±0 15	20‖	30	. . . .
	+142	−30 0			. .	0 13±0 06	40?	4 4	. . . .
	+106?	−22 4			. . .	0 10±0 07	. . .		. .
	+ 5	− 1 1			. .	3 0 + ∞ −0 7	62	190	. . . . .
	− 73	+15 4		.	. . .	0 45±0 15	36	15	. . . . .
	−105#	+22 2	.		. . . .	0 25±0 07	60	8 8	. . . . .
3C 123	− 22	+ 4 6	.		. . . .	1 65+ ∞ −0 7	28	50	0

* Uncertain because of saturation corrections

† For the single dish, this is the average of the two features listed above, which are too close to separate individual widths and integrated optical depths

‡ This is a broad wing on the profile and may consist of several blended features Thus the estimated width has little significance

§ With the single dish, this feature appears as if it might be double.

‖ The width at half optical depth The shape is very different from the usual The core gives a much narrower width.

A broad wing with no symmetrical shape; the estimated width has little significance.

(1958) finds a small component on the slope of the deep line at +180 kc/sec. We find indications of asymmetry in the slope near the bottom of the line at +4 kc/sec, which suggests that there may be fine structure in this feature. An observation with a narrower band width would probably decide this question.

The most striking difference between the single-dish and interferometer profiles is the almost infinite optical depth in the line at +229 kc/sec as observed with the single dish. This was investigated with some care; several records were averaged together in an attempt to detect the residual radiation from the source. One of these records is shown in

TABLE 3

ADDITIONAL FEATURES OBSERVED ONLY WITH THE SINGLE DISH

Source	Freq. (kc/sec)	Vel. (km/sec)	Max τ	Width	Int. τ	r (kpc)
CTB 31	+ 10?	− 2.1?	0 31?±0 4	?	?	0
	− 23	+ 4 9	1 5 $^{+\infty}_{-0\ 7}$	33	51	0 9
CTB 39.....	− 20	+ 4 2	0 60 ±0 35	61	36	0 (16 7)
	+ 27	− 5.7	1 5 $^{+1\ 0}_{-0\ 6}$	19	39	0.8 (15 3)
W22.....	− 54	+11.4	1 65 $^{+\infty}_{-0.4}$	18	35	. .. .
	− 23	+ 4.9	2 4 $^{+\infty}_{-1\ 0}$	15	46	....
	+ 6	− 1 3	3 0 $^{+\infty}_{-1\ 5}$	20	75	.....
	+ 60	−12.7	0 93 ±0.25	21	20	.. ..
W43.....	− 58	+12.2	2 2 $^{+\infty}_{-1.0}$	23	56	1 0, 14 2
	−103?	+21 7?	0 20 ±0 25	?	?	1.6, 13 6
	−396	+83 6	0 65 $^{+0.7}_{-0\ 4}$	50	33	5.3, 9 9
	−445	+93 9	0 56 $^{+0\ 7}_{-0\ 4}$	60	29	5 9, 9 3
W51.....	− 34	+ 7.2	>1 5	<12	29?	0 4, 10 3
	− 60	+12 7	1 0 $^{+0\ 8}_{-0\ 4}$	28	33	0 7, 10 0
	−225	+47 5	0 80 $^{+0\ 6}_{-0\ 4}$	26	22	3 2, 7 5
	−260	+54.9	0.55 $^{+0\ 5}_{-0\ 3}$	27	16	4.4, 6 3
W75...	− 15	+ 3.2	.....	≈50	.. . ..	0 8, 1 6
	− 54	+11.4	....	≈40	. . .	1 2

Figure 2, *c*. After the small corrections for imperfect image rejection by the cavity and for the finite band width had been applied, the remaining contribution from Cas A was found to be −0.008 ± 0.012 of the unabsorbed source. This indicates essentially infinite optical depth. Even allowing an error of one and one-half times the probable error, the optical depth is greater than 4.7. However, with the interferometer, the optical depth is observed to be 3.41 ± 0.4. That the interferometer profile does not go to zero at the bottom of the deep line is shown quite clearly in the record reproduced in Figure 4. This is not an instrumental effect, as the same or identical cavities and filters were used with the interferometer as with the single dish.

The discrepancy cannot be explained in terms of resolution of the source, as the source still had 75 per cent of its unresolved intensity. This, then, must be an effect of neighboring background at this frequency which is resolved out by the interferometer. The most likely explanation, due to Bolton, is that there is a cold cloud in the antenna beam which

is being resolved out by the interferometer and that this cloud is probably causing absorption in both the source and the background radiation. In order that it may be resolved by the interferometer, it must be greater than about 7′ in size, and, in order that its narrow line should not stand out in the emission spectrum nearby, its angular size must be somewhat smaller than the beam width of the single dish. This requires its diameter to be not greater than about 30′. Taking a diameter of 20′ and a distance, corresponding to the velocity, of 3.5 kiloparsecs, we find the size to be about 20 parsecs, or roughly of the same order as that estimated from the optical interstellar lines (van de

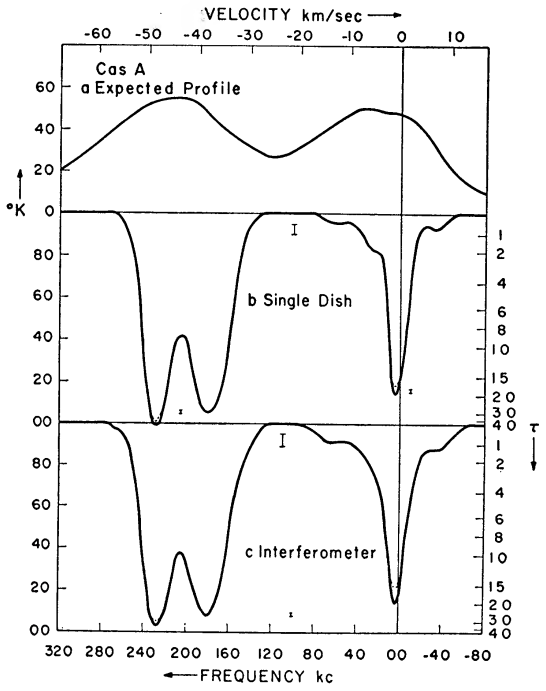

FIG. 6.—The expected profile and the derived absorption profiles for Cassiopeia A, showing the differences between single-dish and interferometer measurements. Single-dish beam width was 35′, and interferometer lobe separation was 12′ east-west. The expected profile only (*top*) is in degrees Kelvin. The absorption profiles are normalized with respect to the unabsorbed source intensity. The uncorrected absorption profile is shown as a dotted line where band-width corrections are appreciable. Where several error bars are indicated, each applies to the portion of profile at about the same height.

Hulst 1958). The cloud causes a drop in the main beam temperature of the single dish of about 9° K. Assuming this drop to be due to the cloud alone, it must have a temperature of less than 60° K. If, however, the observed drop is due only to a large vacant space in the interstellar hydrogen, the temperature in the cloud could be somewhat higher. If we take the temperature to be 100° K, there are 2.9×10^{21} atoms/sq cm, which in a 20-parsec cloud is 47 atoms/cc. Alternatively, if the temperature is only 50° K, these figures become 1.5×10^{21} atoms/sq cm and 24 atoms/cc, respectively.

The same argument can be advanced for the other deep line in the Perseus arm, where we again find a difference between the residual interferometer and single-dish intensities. For the deep line in the Orion arm, however, the optical depths measured with the single dish and with the interferometer are almost exactly the same. This implies either that the absorbing cloud is at much the same temperature as the nearby background emission or, because of its small distance, that it is so large that it fills several beam widths and the edges slope off so gradually that they are not noticed. Both causes may contribute.

b) Cygnus A

Because our present observations were primarily concerned with the measurement of features of large optical depth, the weak lines in Cygnus A were observed only with low accuracy. The absorption profiles are shown in Figure 7. The difference between the single-dish and the interferometer results are not clearly significant. Using the interferometer, the feature at 345 kc/sec appears weaker than when it is observed with a single dish. The feature at 55 kc/sec, however, is stronger when observed with the interferometer. These differences, if real, can be explained on the basis that the first is caused by a cloud of beam-width size which is colder than the background, the second by one which is hotter than the background.

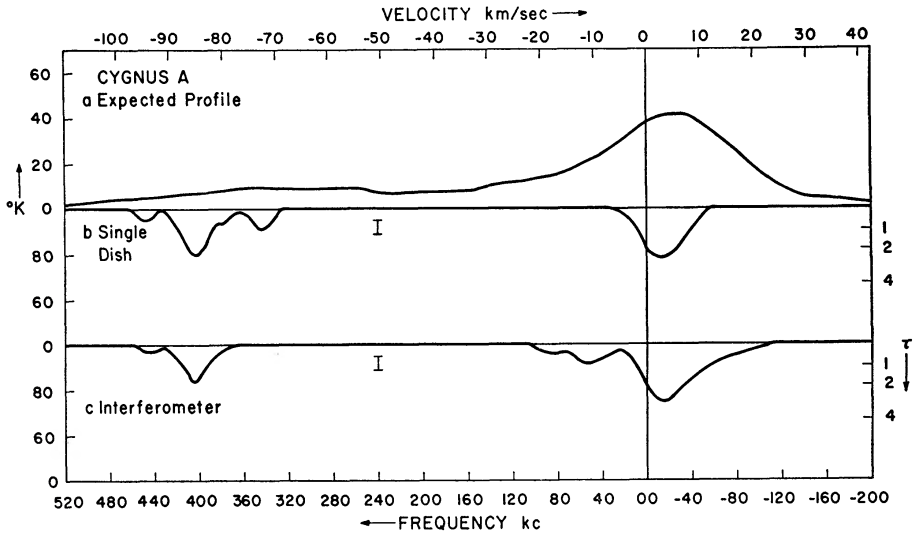

FIG. 7.—The expected profile and the derived absorption profiles for Cygnus A, showing the differences between single-dish and interferometer measurements. Single-dish beam width was 35′, and interferometer lobe separation was 12′ east-west. The expected profile only (*top*) is in degrees Kelvin. The absorption profiles are normalized with respect to the unabsorbed source intensity.

The total integrated optical depth of the features in this source is much less than for any of the other sources near the galactic plane. This is undoubtedly related to the fact that at optical frequencies there is a hole in the galactic absorption at about the position of the Cygnus source.

c) The Crab Nebula

The distance to the Crab Nebula is well known from optical measurements to be about 1100 parsecs. Thus, although their location near the anticenter prohibits getting kinematical distances for the clouds causing the features, their distance has a rather small upper limit. The profiles are presented in Figure 8. The most striking features are the sharp and narrow line at −48 kc/sec and the broader feature at about −15 kc/sec. The changes in detail in the latter feature between the interferometer and single dish may not be significant. The single-dish observations suggest that the line is doubled with components at −10 and −20 kc/sec, but the difficulty of resolving two such closely spaced components is such that one could not estimate a width or maximum optical depth reliably for each component separately. The feature observed with the interferometer at a frequency of −28 kc/sec is probably real, but again it is difficult to separate from the nearby strong features.

In several places in this profile we seem to see fine structure with widths less than about 15 kc/sec. The deep, narrow line at −48 kc/sec appears to have a width of only 12 or 13 kc/sec. These widths are almost compatible with the thermal Doppler broadening of the atomic hydrogen. The half-width of the thermally broadened hydrogen line is 0.215 $T^{1/2}$ km/sec or 1.02 $T^{1/2}$ kc/sec. Thus a line formed in hydrogen at 100° K would have a half-width of 10.2 kc/sec. With features so sharp, the profile becomes somewhat uncertain because of the large band-width corrections. However, the differences between the single-dish and interferometer profiles are real, as the same filters were used for the two methods of observation and there is consequently no difference in the rather uncertain band-width correction to be applied to the lines.

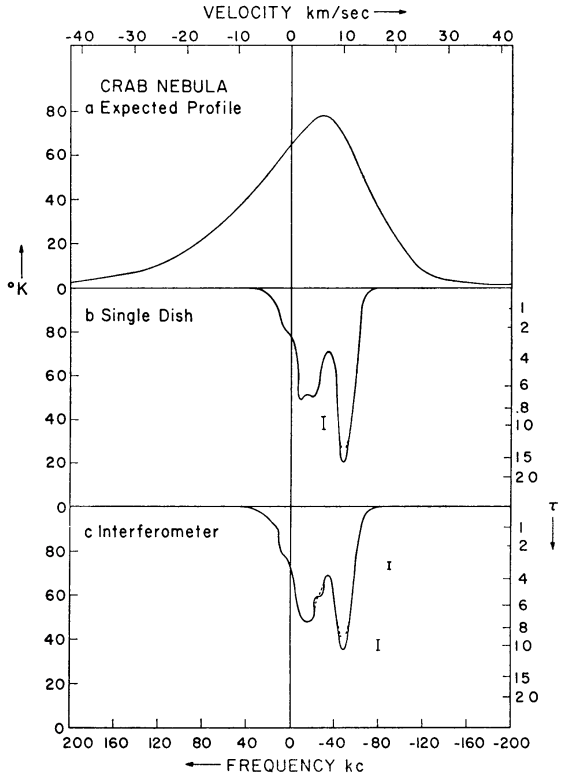

FIG. 8.—The expected profile and the derived absorption profiles for the Crab Nebula, showing the differences between single-dish and interferometer measurements. Single-dish beam width was 35′, and interferometer lobe separation was 12′ east-west. The expected profile only (*top*) is in degrees Kelvin. The absorption profiles are normalized with respect to the unabsorbed source intensity. The uncorrected absorption profile is shown as a dotted line where band-width corrections are appreciable Where several error bars are indicated, each applies to the portion of profile at about the same height.

In this case also, there is probably a cold cloud of about beam-width size which causes the antenna temperature of the area of the source to be about 12° K cooler than the surrounding area. We may argue in the same way as we did for the deep line in Cas A. As the distance cannot be greater than 1100 parsecs, the diameter of a cloud 20′ in extent would be only 6 parsecs. If it were at a temperature of 50° K, there would be 3.2×10^{20} atoms/sq cm, or 16 atoms/cc, numbers very similar to those obtained for Cas A.

d) Orion Nebula

The single-dish profile in Figure 9 appears to have two components, one at −19 kc/sec and one at +14 kc/sec, with maximum optical depths of 1.27 and 0.36, respectively. On

the other hand, the interferometer profile appears to consist of several very narrow components. The interferometer indicates that much more of the source is absorbed than is suggested by the single dish. It should be noted that the observed single-dish results would be obtained from the interferometer profile if the component at −24 kc/sec were decreased in optical depth by 1.2 and the other components kept much the same. If we call upon the same simple model to explain these observations as we did to explain those of the other sources, then the −24 kc/sec feature must be caused by a bright cloud of beam-width size.

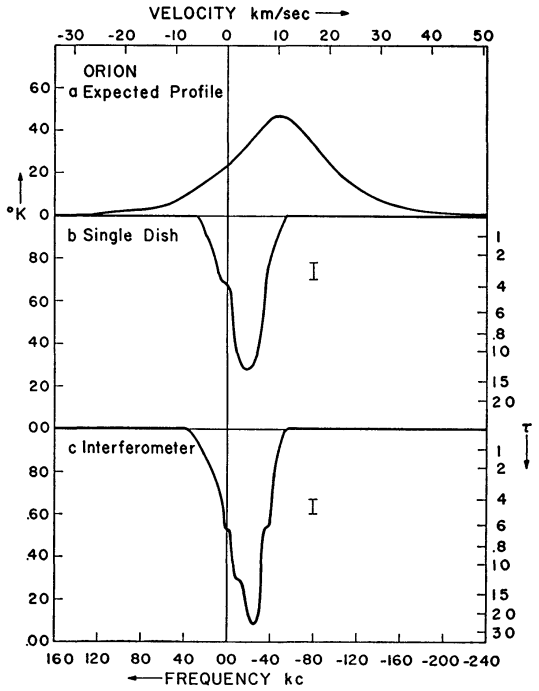

FIG. 9.—The expected profile and the derived absorption profiles for the Orion Nebula, showing the differences between single-dish and interferometer measurements. Single-dish beam width was 35′, and interferometer lobe separation was 12′ east-west. The expected profile only (*top*) is in degrees Kelvin. The absorption profiles are normalized with respect to the unabsorbed source intensity.

The difference between the single-dish and the interferometer profiles corresponds to an increase in single-dish antenna temperature of 8° K. Added to the emission temperature in that direction, this gives a minimum temperature of 55° K for the bright cloud. This cloud must be very much smaller and denser than those producing a related effect in Cas A. As the distance cannot be more than 500 parsecs, the cloud must be smaller than about 5 parsecs in diameter, and its density must be at least 50 atoms/cc.

It is interesting to note the extreme narrowness of the features in the interferometer profile. Still further resolution into fine structure is suggested at the limit of the frequency resolution of our observations. The fortuitous resolution of an apparently smooth feature into narrow components suggests that, in this case at least, the clouds consist of small wisps of the order of size of a few minutes of arc, moving with a velocity of a few kilometers per second with respect to each other and internally broadened only by thermal motions.

e) Omega Nebula

As the Omega Nebula is rather large, part of the changes between the interferometer and the single-dish profiles may be due to the resolution of the source. The fringe visibil-

ity is down to about 0.36 at a spacing of 300 wavelengths. The absorption profiles are presented in Figure 10. The most obvious features are the very strong ones at −34 and at −100 kc/sec. There is a great deal of barely resolved detail in the profile. Four lines are clearly seen, and two more are suggested. The single-dish profile suggests a possible doubling of the feature at −34 kc/sec. These components are not narrow, as in the case of the Crab and Orion Nebulae, having widths of the order of 20 or 30 kc/sec.

The −100 kc/sec line is much weaker with the interferometer than with the single dish. The difference is of the order of 0.15 of the source intensity and can be explained on

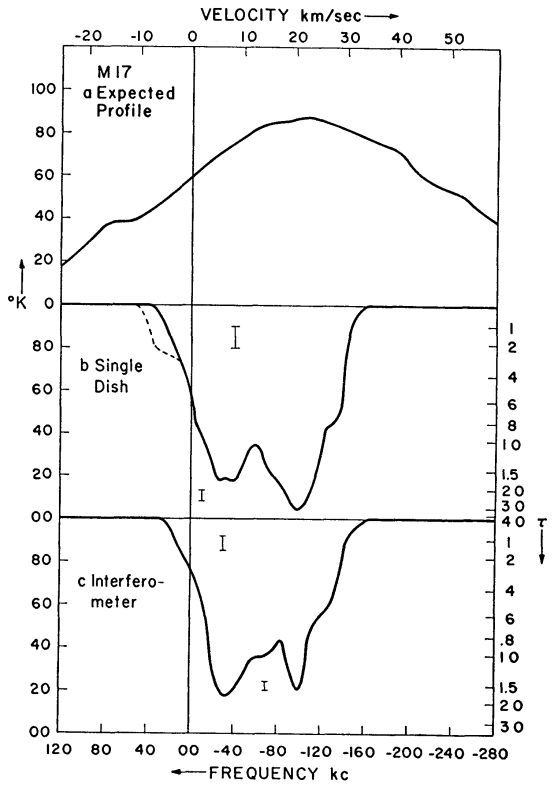

FIG. 10.—The expected profile and the derived absorption profiles for the Omega Nebula, showing the differences between single-dish and interferometer measurements Single-dish beam width was 35′, and interferometer lobe separation was 12′ east-west. The expected profile only (*top*) is in degrees Kelvin. The absorption profiles are normalized with respect to the unabsorbed source intensity. Where several error bars are indicated, each applies to the portion of profile at about the same height.

the basis of resolution; however, this would require that the radiation from that part of the source resolved out by the interferometer be almost totally absorbed. If the above anomalies, corresponding to a single-dish antenna temperature of about 9° K, are caused by resolution of the cloud and not the source, they would indicate a cloud temperature of not more than 75°. The kinematical distance is 2.1 kiloparsecs. At that distance a 20′ cloud would have a diameter of 12 parsecs, and at a temperature of 50° K there would be 5.6×10^{20} atoms/sq cm, or 15 atoms/cc. It should be noted that the line as seen with the interferometer is somewhat narrower than as seen with the single dish. This probably implies that there are large-scale motions in the cloud, with a typical length of at least 5′ or 3 parsecs.

From the absorption profile of the source we may estimate the distance. The last component of the absorption is situated at about −124 kc/sec, corresponding to a distance of

2.6 kiloparsecs, in the Sagittarius arm. We thus conclude that the Omega Nebula probably lies in this arm and is at a distance of not less than 2 kiloparsecs and probably not more than 4 kiloparsecs. Of all the nearby early-type stars listed by Sharpless (1959) and by Stephenson and Hobbs (1961), only one has a known photometric parallax, and its distance is only 660 parsecs, so we may conclude that this is undoubtedly a foreground star and that the actual nebula is considerably more distant.

f) Sagittarius A

The observations of Sagittarius A are presented in Figure 11. Our single-dish observations did not extend beyond +100 kc/sec. The two prominent features in this spectrum are the very deep line at zero velocity and the absorption line caused by the hydrogen in the 3-kiloparsec arm (Rougoor and Oort 1958, 1960) at a frequency of +256 kc/sec. It is very difficult to find the expected profile in the case of the zero-velocity line, because of the cold cloud in front of the source, first discovered by Heeschen (1955). As we have not determined the expected profile ourselves, we reproduce Muller's diagram from the Paris Symposium. The top curve (*dotted*) is a provisional expected profile. The bottom curve is the observed profile found by Muller at the position of the Sagittarius source (Fig. 12).

Our profile is depicted as going negative, since, when we observe the source with the d.c. radiometer, the source actually appears negative, having about the same angular diameter and about the same position as the continuum source. If we reduce these records by the same procedure as that adopted for the other sources, we get negative values for the antenna temperature contributed by the source. A right-ascension drift-curve across the source near zero velocity is reproduced in Figure 13. This was taken with the d.c. radiometer, and a drop in the record indicates an actual decrease in antenna temperature. This negative source is not real but must be explained in terms of incorrect interpolation of the expected profile from the surrounding regions. However, we have drawn the negative curve to make these observations compatible with those of the other sources observed.

Because of the comparatively large distance to the Sagittarius source and since the features due to clouds in circular motion would be superimposed at zero velocity, there may be several clouds contributing to the wide feature. The brightness temperature at the position of the source at zero velocity is probably no greater than 80° K, and this implies that the hydrogen causing the absorption is at least as cold.

The feature at +256 kc/sec is also extremely interesting, as it is much narrower than the single-dish measurements made by Muller (1956) and by Rougoor and Oort (1960) suggest. According to Rougoor and Oort, the line has an optical depth of 0.5 and a width of 50 kc/sec. Our measurements indicate a maximum optical depth of 1.05 and a width of, at most, 20 kc/sec. The width quoted is the full width at half-maximum optical depth and does not have quite the same significance as the other widths given, since the shape of this line is more nearly a dispersion profile than a Gaussian. If only the core of the line is examined, it appears even narrower than the 20 kc/sec quoted. The broad wings could be explained on the basis of radiation from the extended source which is not completely resolved out. The difference in width of the two profiles indicates that there is large-scale motion in the hydrogen, with a typical length of at least 10′ or 15 parsecs. This could be caused by the change of projected expansion velocity across the face of the source. Further investigation with the interferometer should indicate whether this motion is systematic or random.

g) Weak Sources

In addition to the sources discussed above, we have observed various other sources, with the single dish only. These were, for the most part, much weaker than the sources dealt with above, or had rather larger angular sizes. The results are presented in Figures 14–19 and in Table 3. The expected profiles, except for W51, were obtained by interpola-

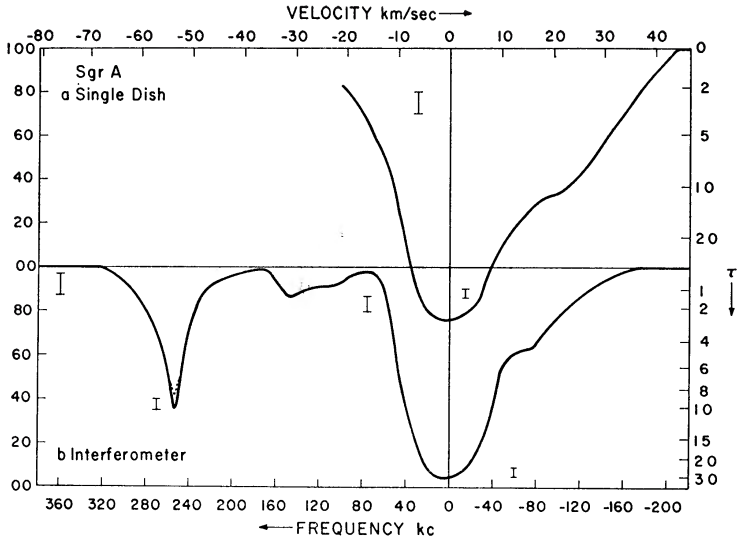

FIG. 11.—Absorption profiles of Sagittarius A taken with the single dish (*top*) and the interferometer (*bottom*).

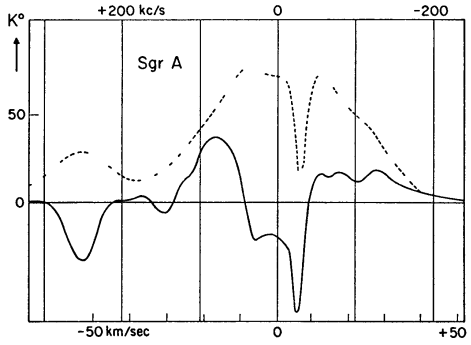

FIG. 12.—Profiles in the direction of Sagittarius A, reproduced from Muller (1958) by kind permission of the publisher. The dotted curve is a provisional expected profile, and the lower trace the actual observed profile at the position of the source.

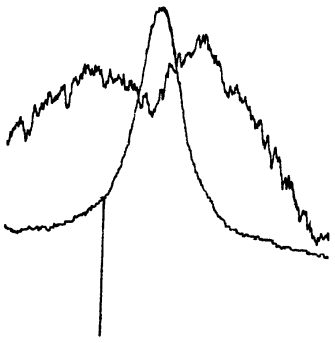

FIG. 13.—A right-ascension drift-curve across Sagittarius taken with the d c. receiver. The narrow-band filter was tuned to a frequency close to zero velocity, and its output actually drops at the position of the source.

tion in the Leiden (Muller and Westerhout 1957) or Sydney (Kerr, Hindman, and Gum 1959) catalogues.

The very-small-diameter source 3C 123 has been observed with the interferometer only. The single-dish results could differ only by the incorrect interpolation of the expected profile. It would be very difficult to obtain a single-dish profile because of the low antenna temperature (5° K) produced by the source. This source was observed primarily to indicate how weak a source the interferometer could conveniently detect in absorption.

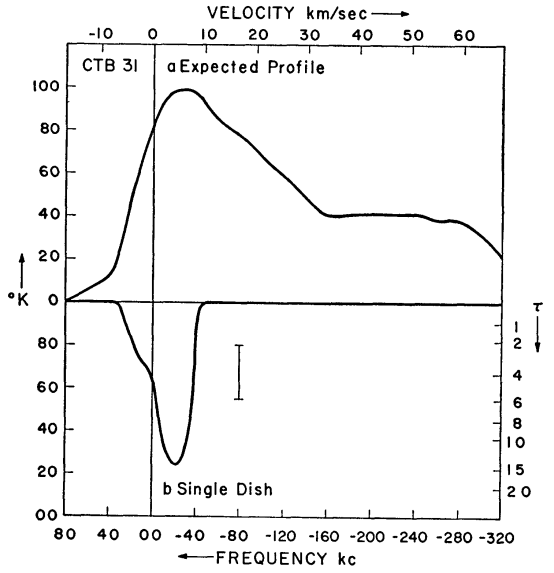

FIG. 14.—The expected and single-dish absorption profile for CTB 31 (CTB numbers are from Wilson and Bolton 1960).

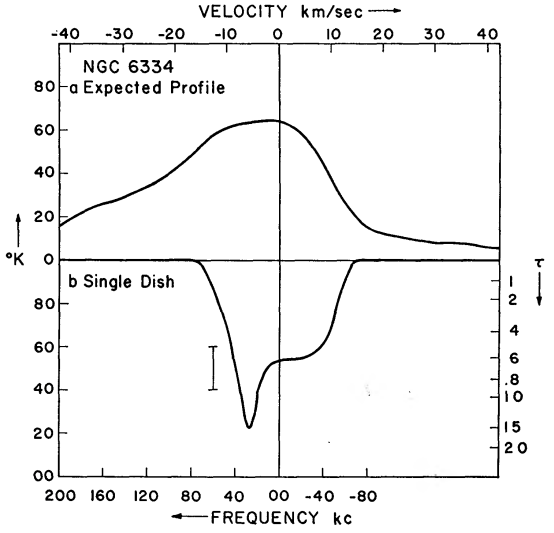

FIG. 15.—The expected and single-dish absorption profile for CTB 39

W51 is an extended source, but it is still possible to sort out the absorption from the local structure. With larger sources, it becomes almost impossible to interpolate the expected profile.

The profile for W75 is very uncertain because of the large angular size of this source. The expected profile must be interpolated over large distances in order to observe regions free from the influence of the source. A drift-curve through the source taken with the switched receiver is shown in Figure 20. The line record is at the top and the continuum trace at the bottom. The size of the source is about 2°. Each of the vertical marks is $1\frac{1}{4}$ minutes of time. One vertical division corresponds to about 1° K on the continuum record

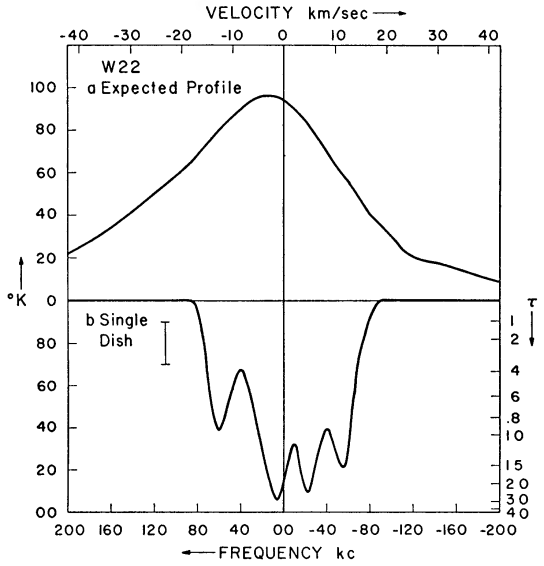

FIG. 16.—The expected and single-dish absorption profiles for W22 (W numbers are from Westerhout 1958).

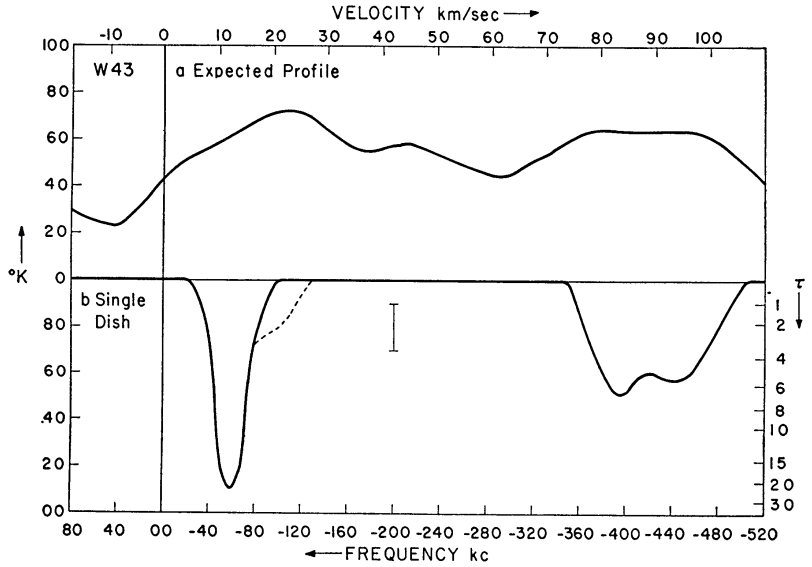

FIG. 17.—The expected and single-dish absorption profiles for W43

and 1.4° K on the line record. That the source appears to be negative at the bottom of the line in Figure 19 is the result of incorrect interpolation of the expected profile. There must be structural features in the local hydrogen of roughly the same order of size as the source and which have a temperature difference of the same order as the brightness temperature of the source. Another large source, Vela X, is so confused that our present data do not allow the sorting-out of absorption and local structure. On all these sources the quoted errors are indicators of the internal consistency of the observations and do not allow for such systematic effects.

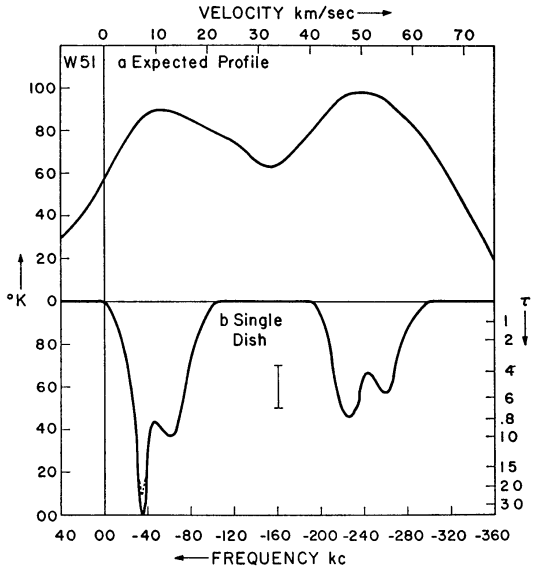

FIG. 18.—The expected and single-dish absorption profiles for W51. The dotted curve shows the absorption profile uncorrected for band width.

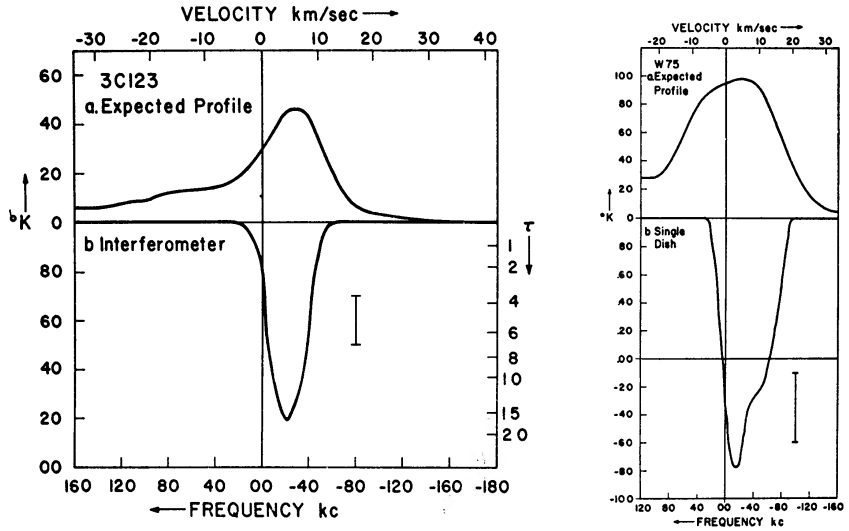

FIG 19.—The two weakest sources seen in absorption. 3C 123 (*left*), a very-small-diameter source, was observed with the interferometer only The very-large-diameter source W75 (*right*) was observed with the single dish only. The source appears negative at the bottom of the line as a result of incorrect interpolation of the expected profile (Fig. 20).

IV. DISCUSSION

We note, first of all, that in those sources which were observed with both the interferometer and single dish the deep lines caused by distant clouds generally appear shallower with the interferometer than with the single dish. On the basis that deep lines tend to be formed by cold clouds, this finds a ready explanation. The many cases we have of small dips in the emission coincident with the source are therefore due to a selection effect. We have used the sources to locate the frequencies of high optical depth and then have very carefully investigated the background at these frequencies, using the interferometer observations to remove the effect of the source, and thus have found the cool cloud. One would also expect to find narrow-band-width, beam-width-sized depressions of about 10° K in the emission in regions other than in front of a source; we have merely used the sources as convenient locators of these depressions.

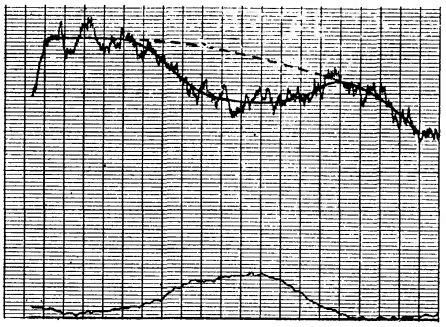

FIG. 20.—A drift-curve showing signs of absorption in W75, taken with the frequency-comparison receiver. The source is about 2° in diameter. If the background is interpolated as shown in the dotted line, the indicated absorption exceeds the source intensity and leads to the unlikely result of Figure 19.

The second general similarity that we wish to point out is the presence of a moderately deep feature near zero velocity in all the sources observed. This suggests that we ourselves may be situated very near, or perhaps within the edge of, one of these very dense clouds. The depths of these features remain the same as viewed with the single dish and with the interferometer, implying that there is no great change in the emission over regions of beam-width size. If we are inside, the cloud must be sufficiently heterogeneous to change from an optical depth of 0.3 to 2 in the 25° between Cygnus A and Cas A.

The data presented in Tables 2 and 3 are probably incomplete for weak source features of optical depths less than 1. However, it is interesting to note the trend. There is a fairly slow rate of decrease in numbers with increasing optical depth. There are about half as many features with optical depths between 2 and 3 as with optical depths between 1 and 2. Our data are not inconsistent with the proposition that such a law—the number halves for every unit increase in optical depth—might hold for optical depths greater than about $\frac{1}{2}$.

The widths have a fairly broad distribution, with a median about 22 kc/sec. There is a scarcity of lines with widths between 35 and 50 kc/sec. This leads one to believe that the wide features would be resolved into blends of narrower features if they were examined with sufficient accuracy. There is a slight tendency for lines of greater integrated optical depth to have a somewhat larger width. This may be real or may be due to the blending of weaker components to form the strong ones, which then appear to have larger widths. If real, it indicates that the variation in optical depth is probably due to mass variation from cloud to cloud, since, if it were due to temperature variation, one would be forced to the unlikely conclusion that colder clouds have greater random velocities.

The space density of these clouds appears highly variable. There are three components

with $\tau > 0.5$ in front of Cas A at about 3.5 kiloparsecs, probably the same number in front of the Crab Nebula at a distance of about 1 kiloparsec, and none in front of Cygnus, which is an extragalactic source. There are probably more of these objects in the spiral arms than in between, but we do not have sufficient data to sort out this effect properly. We shall estimate the space density of these clouds averaged over the local galactic disk. To do this, we discard the many observations of features at about zero velocity, since, as stated above, these features may all be caused by the same cloud, in which case only one should be counted. One is primarily left with two features in Cas A and four in M17 with well-known distances. From these kinematical distances and allowing for the short lengths discarded at the beginning of the path, we find that a line of sight intersects a cloud with $\tau > 0.5$ about once in 1.2 kiloparsecs.

There are four features which appear differently in interferometer and single-dish profiles, whose kinematical distances are well known. Their average distance is 2.3 kiloparsecs. If the difference is due to the absorbing cloud possessing an angular size averaging 20′, the clouds have average diameters of the order of 13 parsecs. Thirteen-parsec clouds spaced at 1.2 kiloparsecs fill about 0.011 of space. It is also interesting to note that the expected distance of the nearest cloud is about 52 parsecs. At this distance the cloud would subtend about 15°.

The average integrated optical depth of the absorption lines with $\tau > 0.5$ is 41 kc/sec. For a cloud temperature of 50° K, this corresponds to 8.0×10^{20} atoms/sq cm, or about 20 atoms/cc for 13-parsec clouds. At this density, each cloud would have a mass of $10^3 M\odot$. This is of the order of 0.2 atom/cc averaged over all space and is a significant portion of the galactic hydrogen. The numbers are uncertain to a factor of 2 at least, because of the uncertainty in the temperature.

V. CONCLUSION

To sum up, we have investigated the absorption spectra of several radio sources with a hydrogen-line interferometer. The results indicate that, while single-dish measurements are correct in broad outline, they are likely to be incorrect in detail, especially near the bottoms of deep lines, because of small-scale variations in the hydrogen emission. These variations tell us the typical sizes of the clouds. With this number we can find gas densities in the clouds. The kinematical distances to the clouds give the densities of the clouds in space. From the kinematical distances, the measured optical depths, and an assumed temperature, we determine the average amount of hydrogen in the clouds and find it to be an appreciable portion of all the hydrogen in the galaxy. We cannot yet answer the question as to whether most of the hydrogen might be present in the form of clouds or even whether the hydrogen seen in absorption is the same as that seen in emission.

More observations are needed in two main directions. With low-noise, solid-state receivers, many weak point sources can be searched for absorption with the interferometer. This will yield much better data on the expected optical depths, space densities, and integrated optical depths. By properly estimating the temperature—perhaps by observing the brightness temperatures of optically thick clouds—these data will give information about the density of hydrogen found in the clouds and may answer the question of whether the emission is due to the cloud hydrogen alone or whether it is necessary to postulate a hot continuum to supply some of the emission.

The second direction is a detailed study of the distribution of the hydrogen across the face of the strong sources. An especially rewarding source to study in this way would be Sgr A, in an attempt to untangle the complicated physics and dynamics at the center of the galaxy. A careful study of Orion A may yield information about the nature of the tiny wisps which appear to be causing the separate parts of the absorption feature. It may perhaps be possible to find the hydrogen temperatures by measuring the thermal broadening of these features. Research in both these directions will continue at the Owens Valley Radio Observatory.

We are indebted to the staff of the Owens Valley Radio Observatory for their help in the course of these investigations, particularly our former director, John G. Bolton, and the acting director, Gordon J. Stanley. We should like to thank Dr. David Morris for taking some of the observations discussed here, and Dr. Alan Moffet for the use of his amplitude-spacing spectra in advance of publication. Our thanks are also due to Professor Rydbeck and Dr. Höglund, of the Chalmers University of Technology, Gothenburg, Sweden, for the expected profiles of the strong sources. This work was supported by the U.S. Office of Naval Research under contract Nonr 220(19). Two of us (B.G.C. and R.W.W.) have held National Science Foundation Predoctoral Fellowships during the course of this work.

APPENDIX I

Interferometric Observations

The response of an interferometer has been described by many authors. The formulae in this section will be based on a discussion by Moffet (1961). We shall use a celestial co-ordinate system (x, y) which reduces to Cartesian co-ordinates in the vicinity of the source. Let the x-axis be parallel to right ascension at the source centroid and the y-axis parallel to declination; x and y are measured in radians and are approximately given by $x = (\alpha - \alpha_0) \cos \delta_0$, $y = \delta - \delta_0$.

The line between the vertices of the two antennas when they are pointed in the same direction is known as the base line of the interferometer and is measured in wavelengths. If the base line is projected onto the (x, y) co-ordinate system, it will have components s_x in the x direction and s_y in the y direction. The response R of the receiver will be

$$R \propto Re\{\exp[i\Psi - 2\pi i s_x \Omega t] \iint T(x, y)\, V_1(x, y)\, V_2(x, y) \times \exp[2\pi i (s_x x + s_y y)]\, dx dy\}, \quad (3)$$

where Ω = sidereal rate, t = sidereal time, Ψ = instrumental phase, $T(x, y)$ = celestial brightness temperature distribution, $V_1(x, y)$ = voltage response of one antenna, and $V_2(x, y)$ = voltage response of the other antenna. When the two antennas are identical and track the same point in the sky, the product $V_1(x, y)\, V_2(x, y)$ can be replaced by the power response of one of the antennas, $A(x, y)$. The integral in equation (3) is now only a slow function of time as s_x and s_y change. If normalized to 1 for $s_x = s_y = 0$, it is known as the "complex visibility function" (Bracewell 1958).

It is clear from expression (3) that if a sufficient number of measurements are made at different values of s_x and s_y, a complete two-dimensional Fourier transform of the function $T(x, y)\, A(x, y)$ can be obtained. This transform can then be inverted to recover the function $T(x, y)\, A(x, y)$ with resolution limited only by the maximum s_x and s_y. For sources much smaller than the antenna beam, $T(x, y)\, A(x, y)$ will be negligibly different from $T(x, y)$.

In the case of hydrogen-line observations, this procedure is complicated by the additional dimension of frequency. The time involved in deriving complete brightness-distribution maps for each frequency may be prohibitive, but useful information can be derived from much simpler observations. At this time, observations have been made using only one base line (300 λ east-west). Projection effects caused variations in s_x and s_y, but the changes were too small to be anything but an inconvenience.

Since the observations are so limited at present, it will be necessary to make two rather strong assumptions. The first is that the structure of the radiation from H I clouds is such that the contribution to the integral in formula (3) from this radiation is negligible. This can come about in either of two ways. Either the individual clouds are so large compared with the lobe spacing that they separately contribute nothing to the integral, or, if they are small enough to contribute, the total flux from each cloud will not be large because of the low surface brightness. The sum of several clouds in the beam contributing at random phases wi l therefore be small. If H I clouds

have a finite size, it is clear that this assumption must be valid for all base lines that are sufficiently large. With this assumption, equation (3) becomes

$$R \propto Re\{\exp\ [i\Psi - 2\pi i s_x \Omega t] \int\int T_s(x, y)\, A\,(x, y) \exp[-\tau(\nu, x, y)] \times \exp[2\pi i(s_x x + s_y y)]\, dx dy\}, \quad (4)$$

where $\tau(\nu, x, y)$ is the optical depth distribution due to all hydrogen between the sun and the source and $T_s(x, y)$ is the source brightness-temperature distribution.

The second assumption is that $\tau(\nu, x, y)$ is constant over the source. With this assumption, formula (4) becomes

$$R \propto \exp[-\tau(\nu)]\, Re\{\exp[i\Psi - 2\pi i s_x \Omega t] \int\int T(x, y)\, A\,(x, y) \times \exp[2\pi i(s_x x + s_y y)]\, dx dy\}. \quad (5)$$

It is seen from formula (5) that the brightness distribution is now independent of frequency and that the absorption profile is independent of s_x and s_y. The absorption profile can be measured by sweeping the frequency of the receiver and measuring the fringe amplitude. If s_x and s_y change during the measurements, corrections can be made by interpolating from the source visibility function measured at frequencies close to, but outside, the absorption range, since $T_s(x, y)$ is a slow function of ν. Of course, after measurements are made at significantly different values of s_x and s_y, the last assumption can be dropped, and the distribution of absorption across the sources can be found by using formula (4).

REFERENCES

Bracewell, R. N. 1955, *Australian J. Phys.*, **8**, 200.
———. 1958, *Proc. I.R.E.*, **46**, 97.
Davies, R. D. 1956, *M.N.*, **116**, 443.
———. 1957, *Radio Astronomy: I.A.U. Symposium*, No. 4, ed. H. C. van de Hulst (Cambridge: Cambridge University Press), p. 71.
———. 1958, *Rev. Mod. Phys*, **30**, 931.
Edge, D. O., Shakeshaft, J. R., McAdam, W. B., Baldwin, J. E., and Archer, S. 1959, *Mem. R. Astr. Soc.*, **68**, 37.
Hagen, J. P., Lilley, A. E., and McClain, E. F. 1955, *Ap. J.*, **122**, 365.
Hagen, J. P., and McClain, E. F. 1954, *Ap. J.*, **120**, 368.
Heeschen, D. S. 1955, *Ap. J.*, **121**, 569.
Hulst, H. C. van de. 1958, *Rev. Mod. Phys.*, **30**, 913.
Kerr, F. J., Hindman, J. V., and Gum, C. S. 1959, *Australian J. Phys.*, **12**, 270.
Lilley, A. E., and McClain, E. F. 1958, *Proc. I.R.E.*, **46**, 220.
McClain, E. F. 1955, *Ap. J.*, **122**, 376.
Moffet, A. T. 1961, in preparation.
Muller, C. A. 1957, *Ap. J.*, **125**, 830.
———. 1958, *Paris Symposium on Radio Astronomy*, ed. R. N. Bracewell (Stanford: Stanford University Press), p. 360.
Muller, C. A., and Westerhout, G. 1957, *B.A.N.*, **13**, 151.
Radhakrishnan, V. 1960, *Pub. A.S.P.*, **72**, 296.
Radhakrishnan, V., and Bolton, J. G. 1960, *A.J.*, **65**, 498.
Radhakrishnan, V., Morris, D., and Wilson, R. W. 1961, *A.J.*, **66**, 51.
Rougoor, G. W., and Oort, J. H. 1958, *Paris Symposium on Radio Astronomy*, ed. R. N. Bracewell (Stanford: Stanford University Press), p. 416.
———. 1960, *Proc. Nat. Acad. Sci.*, **46**, 1.
Schmidt, M. 1956, *B.A.N.*, **13**, 15.
Sharpless, S. 1959, *Ap. J. Suppl.*, **4**, 157.
Stephenson, C.B., and Hobbs, R. W. 1961, *A.J.*, **66**, 186.
Westerhout, G. 1958, *B.A.N.*, **14**, 215 (No. 488).
Williams, D. R. W., and Davies, R. D. 1954, *Nature*, **173**, 1182.
Wilson, R. W., and Bolton, J. G. 1960, *Pub. A.S.P.*, **72**, 331.